A Hard Medium Survey with the ASCA GIS: the (2-10 keV) Number Counts Relationship

I. Cagnoni[1,2,3] , R. Della Ceca[4,5] and T. Maccacaro[4,6]

[1] *Università degli Studi di Milano, Via Celoria 16, 20133, Milano, Italy*

[2] *Present address: Harvard-Smithsonian Center for Astrophysics, 60 Garden Street, Cambridge, Massachusetts 02138, USA*

[3] *E-mail: ilaria@alessandro.harvard.edu*

[4] *Osservatorio Astronomico di Brera, Via Brera 28, 20121 Milano, Italy*

[5] *E-mail: rdc@brera.mi.astro.it*

[6] *E-mail: tommaso@brera.mi.astro.it*

ABSTRACT

In this paper we report the first results on a medium survey program conducted in the 2-10 keV energy band using data from the GIS2 instrument onboard the ASCA satellite.

We have selected from the ASCA public archive (as of February 14, 1996) 87 images which are suitable for this project. Sixty serendipitous X-ray sources, with a signal-to-noise ratio greater than 3.5, were found. The 2-10 keV flux of the detected sources ranges from $\sim 1.1 \times 10^{-13}$ ergs cm^{-2} s^{-1} to $\sim 4.1 \times 10^{-12}$ ergs cm^{-2} s^{-1} .

Using this sample we have extended the description of the 2-10 keV LogN(>S)–LogS to a flux limit of $\sim 6.3 \times 10^{-14}$ ergs cm^{-2} s^{-1} (the faintest detectable flux), i.e. about 2.7 orders of magnitude fainter than the Piccinotti et al. (1982) determination. The derived number-flux relationship is well described by a power law model, $N(> S) = K \times S^{-\alpha}$, with best fit values $\alpha = 1.67 \pm 0.18$ and $K = 2.85 \times 10^{-21}$ deg^{-2}.

At the flux limit of the survey about 27 % of the Cosmic X-ray Background in the 2-10 keV energy band is resolved in discrete sources. A flattening of the number-flux relationship, within a factor of 10 from the flux limit of the present survey, is expected in order to avoid saturation.

The implications of these results on the models for the origin of the hard X-ray background are briefly discussed.

Subject headings: diffuse radiation - surveys - X-rays:galaxies - X-rays:general

1. Introduction

The origin of the Cosmic X-ray Background (CXB), discovered almost 35 years ago (Giacconi et al., 1962), represents one of the long-standing problem of modern cosmology (see the reviews by Fabian and Barcons, 1992; Setti and Comastri, 1996).

The very small deviation from a blackbody shape of the cosmic microwave background spectrum seems to have put to rest the suggestion that a significant fraction of the CXB is due to truly diffuse emission from a hot intergalactic medium (Mather et al., 1994). Therefore only the alternative interpretation, the discrete sources origin, is left.

X-ray surveys provide a powerful tool to study the nature and properties of the classes of X-ray emitters which produce the CXB. In the soft X-ray energy band ($E < 2$ keV), where grazing incidence focusing optics have been used, deep surveys conducted with the ROSAT observatory (Hasinger et al., 1993; Branduardi-Raymont et al., 1994; Vikhilin et al., 1995) have revealed a surface density of X-ray sources of ~ 415 deg^{-2} at a flux limit of 2.5×10^{-15} ergs cm^{-2} s^{-1} (0.5 – 2.0 keV), contributing $\sim$ 60-65 % of the CXB in the same energy band. The differential log(N)–log(S) can be described (see e.g. Hasinger et al., 1993) by a broken power-law model with slope ~ 1.85 for $S \lesssim 2.2\times10^{-14}$ ergs cm^{-2} s^{-1} and ~ 2.6 for $S \gtrsim 2.2 \times 10^{-14}$ ergs cm^{-2} s^{-1} . At brighter fluxes a good agreement is found with the surface density previously obtained using data from the *Einstein* Observatory (Primini et al., 1991; Gioia et al., 1990).

Spectroscopic observations of the ROSAT sources along with the results obtained by the *Einstein* Observatory Extended Medium Sensitivity Survey identification program (EMSS; Gioia et al., 1990; Stocke et al., 1991; Maccacaro et al., 1994) have allowed us to clarify the nature and composition of the sources which shine in the soft X-ray sky.

Broad Line AGNs constitute the majority of the soft X-ray sources at the fluxes actually sampled: they represent $\sim 50\%$ of the sources in the EMSS ($< z > \simeq 0.4$) and $\sim 50-60\%$ of the ROSAT sources with $S \gtrsim 5-6 \times 10^{-15}$ ergs cm^{-2} s^{-1} ($< z > \simeq 1.5$; Shanks et al., 1991; Boyle et al., 1993;1994;1995; Jones et al., 1997).

Clusters of galaxies are the next most numerous class of extragalactic sources in bright X-ray surveys. At $S \geq 1 \times 10^{-13}$ ergs cm^{-2} s^{-1} , for example, they represent $\sim 13\%$ of the sources in the EMSS. However they become less important as one moves to fainter fluxes (Rosati et al., 1995).

An important minority ($\sim$ 10%) of the ROSAT sources are spectroscopically identified with X-ray luminous galaxies, consisting of both early-type and Narrow Emission Line Galaxies (Griffiths et al., 1995; 1996). According to their cosmological evolution properties (Griffiths et al., 1996) these objects could become increasingly more important at fainter fluxes and could constitute a significant fraction of the largely unidentified sources present at the ROSAT deep surveys flux limit. The real nature of these objects (obscured AGN ? starburst galaxies ?) is at the moment unclear.

Based on studies on the cosmological properties of the known classes of objects it is now evident that their combined contribution to the soft CXB is approaching 100 per cent (see e.g. Broad Line AGN: Boyle et al., 1993;1994; Jones et al., 1997; clusters of galaxies; Rosati et al., 1995; X-ray luminous galaxies: Boyle et al., 1995; Griffiths et al., 1995;1996).

In contrast, our knowledge of the nature and composition of the sources which produce the 2-10 keV CXB, closer to where the bulk of the energy density resides, is quite scanty. Before ASCA (acronym for *Advanced Satellite for Cosmology and Astrophysics*), the surveys in this energy range were made using passively collimated X-ray detectors. These instruments were able to measure accurately the CXB spectrum (which is remarkably well fitted by a thermal bremsstrahlung model with a temperature of the order of 40 keV, see Marshall et al., 1980; Gruber et al., 1992) but, because of the limited spatial resolution, they were only able to resolve the brightest X-ray sources which represent only a small fraction ($< 5\%$) of the CXB.

The only statistically complete and large sample of X-ray sources in the 2-10 keV energy band was obtained from the A-2 experiment on HEAO-1 (Piccinotti et al., 1982). This sample is composed of 85 sources (excluding the LMC and SMC), brighter than $\sim 3.1 \times 10^{-11}$ ergs cm^{-2} s^{-1} , found in ~ 8.2 *sr* of the sky at $|b| > 20^o$. Of the 62 sources of extragalactic origin about half are AGN and half are cluster of galaxies.

Source counts down to a flux of $\sim 8 \times 10^{-12}$ ergs cm^{-2} s^{-1} were obtained by Kondo et al., 1991 using data from the *Ginga* satellite. A small sample of 11

sources was derived from the analysis of 383 square degrees.

The *Ginga* fluctuations analysis (Warwick and Stewart, 1989; Butcher et al., 1997) extend the study of the number-flux relationship to a flux of the order of $\sim 10^{-13}$ ergs cm^{-2} s^{-1} . However these studies are model dependent (the spectral and clustering properties of the sources have to be assumed) and do not give direct indications on the intrinsic nature of the X-ray emitters which are responsible of the CXB.

The so called "spectral paradox", i.e. none of the single classes of known X-ray emitters is characterized by an energy spectral distribution similar to that of the CXB, further complicates the situation.

Given this frustrating situation, a method to derive the contribution to the hard CXB of the different classes of X-ray sources through population synthesis models was developed (i.e. by using their average broad-band spectral properties folded with their cosmological evolution properties determined in the soft X-ray energy band). Among the proposed classes of X-ray emitters that could be important for the production of the hard CXB there are reflection dominated AGN (Fabian, 1989; Zdziarski et al., 1993 and reference therein), strongly absorbed AGN (Setti and Woltjer, 1989; Madau Ghisellini and Fabian, 1994; Comastri et al., 1995) and starburst galaxies (Griffiths and Padovani, 1990).

It is clear that a direct measurement, through selection of a sample of hard X-ray emitters, is therefore crucial to test competing models.

The ASCA satellite is carrying the first imaging instrument in the 2-10 keV energy band. This gives us the possibility to determine the surface density of hard X-ray selected sources to $\lesssim 10^{-13}$ ergs cm^{-2} s^{-1} directly from the source counts and to clarify the nature of the X-ray emitters which are responsible of the hard CXB through optical spectroscopic follow up observations.

In this paper we report preliminary results on a medium survey program in the 2-10 keV energy range using data from the GIS2 instrument onboard the ASCA observatory. The paper is organized as follows. In section 2 we discuss the criteria for the selection and construction of the images used, for the selection of the sources and for the definition of the sky coverage. In section 3 we report the main result obtained so far: the number counts relationship, derived **directly from source counts**, down to a flux limit of $\sim 6.3 \times 10^{-14}$ ergs cm^{-2} s^{-1} . We compare this Log(N>S)–LogS with previous results from HEAO-1 and *Ginga*, with new results obtained from other groups using ASCA deep survey fields and with the extrapolation of the Log(N>S)–LogS from the soft X-ray energy band. Finally in section 4 a discussion and conclusions are presented.

2. Selection Criteria and Data Analysis

ASCA (Tanaka, Inoue and Holt, 1994; Serlemitsos et al., 1995) was launched on 1993 February 20 by the Japanese Institute for Space Astronautical Science. The focal plane instrumentation consists of two Solid-State Imaging Spectrometers (hereafter SIS0 and SIS1 or in general SIS) and two Gas Imaging Spectrometers (hereafter GIS2 and GIS3 or in general GIS), simultaneously operating.

For the purpose of this survey we have decided to use the GIS2 instrument for the following reasons:

a) the GIS has a circular field of view of $\sim 50'$ diameter, ~ 4 times larger than the SIS field of view of $\sim 22' \times 22'$ (when used in 4 CCD mode). Furthermore only a limited number of ASCA observations were made with the SIS in the 4-CCD mode option;

b) for energies above ~ 5 keV the effective area of the GIS is larger than the effective area of the SIS;

c) the GIS2 detector has a larger area uncontaminated from a high Non-X-Ray background than the GIS3 (see the Announcement of Opportunity EAO_1; ASCA guest investigator programme).

2.1. ASCA Field Selection and GIS2 Cleaning Parameters

The ASCA public data considered here were extracted from the public archive (as of February 14, 1996).

We have excluded from the survey those fields centered on:

1) $|b| < 20$

2) targets in the Large and Small Magellanic Clouds

3) very bright (see section 2.4) and/or extended targets, e.g. supernovae remnants, very rich and nearby clusters of galaxies;

4) groups and/or associations of targets, e.g. groups of nearby galaxies, star clusters or stellar association.

All these selection criteria were applied to avoid regions of high Galactic absorption and high stellar

density, to dismiss images where the background map (see Section 2.2) could not be produced reliably and to prevent including in the survey sources not truly serendipitous (e.g. physically related to the target). We have also excluded from the analysis those images with an exposure time (after the data cleaning, see below) less than 10000 s since their sensitivity is so poor that they do not significantly contribute to the sky coverage of the survey. Finally in the case of two or more overlapping images we have retained only the deepest one.

A total of 87 GIS2 fields (listed in Table 1) survive to these selection criteria.

Image preparation has been performed using version 1.2 of the XSELECT software package and version 3.2 of FTOOLS. Good time intervals were selected by applying standard cleaning criteria, the most relevant being a magnetic cut-off rigidity threshold of 6 (COR_MIN > 6) and a minimum elevation angle of 6 (ELV_MIN > 6). We have also excluded from the analysis periods of time that are within 60 s from the South Atlantic Anomaly passage and within 100 s from the day/night transition passage. Finally, images were extracted in the 2-10 keV energy range, in detector coordinates and considering only the events within 20 arcmin from the detector center. The pixel size of these images is $15'' \times 15''$.

2.2. Source Detection and Selection

To localize and characterize the faint sources contained in the selected fields we need to estimate the underlying background as precisely as possible. A detailed description of the properties of the GIS2 background is reported in Kubo et al., 1994 and Ikebe et al., 1995. In brief the GIS2 background consists of Non X-ray Background (NXB) and Cosmic X-ray Background (CXB); the first one increases from the center to the edge of the detector while the latter one shows an opposite behavior.

After a detailed radial and azimuthal analysis of the background properties in 30 GIS2 images (which do not show evident X-ray sources) we reached the conclusion that the GIS2 background has a structure that is reproduced from image to image. For these reasons we have decided to use the Blank-Sky event files, which include both the NXB and CXB. These Blank-Sky event files have been constructed by the GIS team summing a total of 15 separate pointings of blank fields [1] and have been made publicly available.

In order to match as closely as possible the selection criteria used to extract the survey images we have extracted Blank-Sky images (hereafter BSI) in the 2-10 keV energy band including only the events with a magnetic cut-off rigidity threshold above 6.

We have then applied the following multi-step procedure to each image (hereafter *ima*):

a) a first estimate of the background statistics in *ima* has been determined in 3 boxes (each of size $5' \times 5'$) which do not contain evident X-ray sources. Median values of the mean and standard deviation from these 3 regions have been considered ($\overline{cts}$, σ);

b) $\overline{cts}$ and σ have been used to define the region (hereafter reg_{back}) in *ima* where the counts (per pixel) are $\leq \overline{cts} + 2\sigma$;

c) this region has been used to produce a normalized version of the background map (hereafter *back*) by rescaling the BSI according to:

$$back = BSI \times \frac{Total\ Counts\ in\ ima\ from\ reg_{back}}{Total\ Counts\ in\ BSI\ from\ reg_{back}};$$

We have preferred to normalize in this way the exposure map, rather than by using the exposure time, because from our analysis of the 30 GIS2 images we have found that the background rate can significantly change from image to image in its intensity but not in the overall structure across the field.

d) *ima* and *back* have been then smoothed with a bidimensional Gaussian with $\sigma = 1'$, which is comparable to the "core" of the (XRT+GIS2) PSF;

e) the smoothed version of *back* has been subtracted from the smoothed version of *ima* in order to obtain a background-subtracted image (hereafter *ima-back*);

f) contour plots in *ima-back* have been used to localize the contiguous pixels (hereafter *peaks*) which are 0.5σ above the local mean. The value of 0.5σ has been determined empirically and ensure completeness above the source detection threshold of 3.5 used (see below);

g) net counts, in a circle of 2 arcmin radius around each of these peaks, are computed by subtracting the

[1] Even if these observations do not contain bright X-ray sources, we found evidence of 3 faint sources; these sources have been averaged out by substituting mean values from surrounding areas.

background counts accumulated in *back* from the total counts accumulated in *ima*;

h) sources are accepted as real if the signal-to-noise ratio (S/N), defined as [(net counts / (net counts + background)$^{1/2}$)], is greater than 3.5.

Excluding the sources related to the targets and the targets themselves, a total of 60 X-ray sources satisfy the criteria for the inclusion in the survey.

In Table 2 (not reported in the pre-print version) we report the basic data for the 60 sources in the sample. In particular we list the name, the ASCA ROR where the source was found, celestial (J2000) coordinates, the signal-to-noise ratio, the corrected flux (and its error) and the Galactic N_H along the line of sight. We note that the absolute accuracy of the ASCA attitude solution is of the order of 2 arcmin.

2.3. Correction for vignetting and PSF

In order to obtain the correct flux of the sources we must now consider the position dependent sensitivity of the GIS2 detector. In particular we must take into account: a) the fraction of the source photons falling outside the 2 arcmin circle radius; b) the variation of the sensitivity of the detector as a function of the distance from the optical axis due to vignetting and c) the variation of the (XRT+GIS2) PSF across the field of view. These effects are taken into consideration by the FTOOLS task ASCAARF which is able to produce a position-dependent PSF-corrected effective area of the (XRT+GIS2) combination. In essence the input of ASCAARF is the position x, y (in detector coordinates) and the dimension of the source extraction region dr (in our case a circle with a radius of 2 arcmin).

Using ASCAARF (version 2.64) we have produced a raster scan of the effective area values across the GIS2 field of view and used them (through spectral simulation with XSPEC) to obtain the count rate to flux conversion factors (f_{xy}) relative to each position x, y in the detector. In the spectral simulations we have used a power law model with energy index equal to 0.7, filtered by a Galactic absorbing column density of 3×10^{20} cm^{-2}. The count rate to flux conversion factors are a very weak function of the Galactic absorbing column density along the line of sight (which ranges from 10^{20} cm^{-2} to $8{\times}10^{20}$ cm^{-2} for the present sample) and are accurate to $\pm$15% for all the energy spectral indices in the range 0.5–1.0. The flux of each source has then been computed and is listed in Table 2.

2.4. Sky Coverage

The sky coverage (i.e., the area covered as a function of the flux limit) of the present survey has been determined in the following way. At each position of a raster scan of a given image we have used the corresponding background map to compute the total counts that a source should have had to be detected at the 3.5 S/N level. These counts have been then converted to count rate and then flux using the same conversion factors (f_{xy}) used for the sources.

The area associated with the target has been excluded from the sky coverage computation; to this purpose we have considered as target area the circle defined by the location where the expected counts from the pointed source are $\geq$ 15% of those of the background in the corresponding background map. The circles associated to the targets range between 6 arcmin to 10 arcmin radius. In the case of circles greater than 12 arcmin radius we have excluded the whole field from the survey.

An integral representation of the sky coverage is reported in figure 1.

The raster scan used to compute the sky coverage allows us to estimate the number of expected spurious sources in the survey. The number of background counts in *back* inside a circle of 2 arcmin radius is a function of a) the image exposure time and b) the circle position in the image. The background counts range between 10 and 15 counts for an image with an exposure time of $\sim$ 10 ksec, between 35 and 50 counts for an image with an exposure time of $\sim$ 40 ksec and between 65 and 85 counts for an image with an exposure time of $\sim$ 70 ksec. Considering the extremes of these values, the requirement of S/N = 3.5 implies that a minimum of 19 (39) net counts have to be recorded on top of the 10 (85) background counts. For a Poisson distribution the probability of observing 29 (124) total counts or more when 10 (85) are expected is 7.6×10^{-7} (4.3×10^{-5}). We note that the 4 σ level in Gaussian statistics is $\sim 6 \times 10^{-5}$. The number of resolution elements of this survey is $\sim$ 6000 (total area divided by the detection cell area); thus the number of spurious sources expected is < 0.3.

3. Results

In figure 2 we show (open circles) a non-parametric representation of the number-flux relationship, ob-

tained by folding the sky coverage with the flux of each source. Because we are primarily interested in the extragalactic number-flux relationship we have excluded from the computation two sources (a0341-4353 and a1410+5215) which are suspected to be stars. In the same figure we also report a parametric representation (solid line) of the LogN(>S)–LogS, obtained by applying the maximum likelihood method to the unbinned data (see Gioia et al.,1990 for details on these two representations). The fit has been performed from a flux of $\sim 6.3 \times 10^{-14}$ ergs cm^{-2} s^{-1} (the faintest detectable flux) to a flux of $\sim 10^{-11}$ ergs cm^{-2} s^{-1} . For fluxes brighter than this limit we may not be complete since most of the "bright" X-ray sources were chosen as target of the observations and then excluded, by definition, from the survey. However we note that the space density of sources with flux greater than $\sim 10^{-11}$ ergs cm^{-2} s^{-1} is such that less than 0.2 sources are expected in this survey. We also note that less than 1 source is expected with flux between $\sim 6.3 \times 10^{-14}$ ergs cm^{-2} s^{-1} and $\sim 1.1 \times 10^{-13}$ ergs cm^{-2} s^{-1} (the flux of the faintest detected source).

The LogN(>S)–LogS can be described by a power law model N(>S) = K $\times S^{-\alpha}$ with best fit value for the slope of $\alpha = 1.67$; the 68% and 90% confidence intervals are equal to [1.49;1.84] and [1.38;1.96] respectively (see Table 3). The normalization K is determined by rescaling the model to the actual number of objects in the sample and, in the case of the "best" fit model, is equal to K = 2.85×10^{-21} deg^{-2}. The two dotted lines in figure 2 represent the $\pm$68% confidence intervals on the slope. A consistent "best" fit model is obtained if we consider only the 26 sources detected with a S/N ratio greater than 5 and the corresponding sky coverage ($\alpha = 1.71 \pm 0.26$; K = 8.28×10^{-22} deg^{-2}).

The filled square at $\sim 3 \times 10^{-11}$ ergs cm^{-2} s^{-1} represents the surface density of the extragalactic population in the Piccinotti et al., 1982 sample, corrected for the 20% excess of sources due to the local superclusters (as estimated by Comastri et al., 1995).

The filled triangle at $\sim 8 \times 10^{-12}$ ergs cm^{-2} s^{-1} represents the surface density of X-ray sources as determined by Kondo et al., 1991 using a small sample of 11 sources extracted from the Ginga high Galactic latitude survey.

Finally, the surface densities represented by the filled dots at $\sim 2 \times 10^{-13}$ ergs cm^{-2} s^{-1} and $\sim 4 \times 10^{-14}$ ergs cm^{-2} s^{-1} are preliminary results from an ongoing ASCA survey programs conducted on a more limited area of sky (as reported in Inoue et al., 1996), while the filled dot at $\sim 5 \times 10^{-14}$ ergs cm^{-2} s^{-1} is a recent results obtained by Georgantopoulus et al., 1997 using 3 deep ASCA GIS observations.

Consistent results (at a flux limit of $\sim 6 \times 10^{-14}$ ergs cm^{-2} s^{-1}) are obtained using data from the BeppoSAX deep surveys (P. Giommi, private communication).

Figure 2 shows that we have extended the description of the (2-10 keV) number-flux relationship by a factor $\sim$ 450 with respect to the Piccinotti et al., (1982) determination, with a sample of similar size.

We can now evaluate, directly from the source counts, the contribution of the resolved sources to the 2-10 keV CXB. This contribution is the ratio between the background surface brightness and the emissivity of the objects under study, which is obtained via integration of the observed LogN(>S)–LogS.

In the 2-10 keV energy range the spectrum of the CXB can be described by a power law representation with energy spectral index equal to 0.4 and normalization equal to 8 keV cm^{-2} s^{-1} sr^{-1} keV^{-1} (see the review of Hasinger, 1996), implying a background surface brightness of $\sim$ 32.87 keV cm^{-2} s^{-1} sr^{-1}.

The emissivity of the resolved objects, I_{obj}, is given by

$$I_{obj} = \int_{S_{min}}^{\infty} S \times N(S) dS$$

where S is the source flux, N(S)dS is the differential representation of the number-flux relationship and S_{min} is the limiting flux considered.

Using the LogN(>S)–LogS best fit model (and the $\pm$68 % confidence interval) and $S_{min} = 6.3 \times 10^{-14}$ ergs cm^{-2} s^{-1} (the flux limit of the survey) we obtain $I_{obj} = 8.8^{+0.6}_{-0.2}$ keV cm^{-2} s^{-1} sr^{-1}, which represents about 27% of the 2-10 keV CXB.

We note that our determination of the total intensity produced by the detected sources is *independent* of the intensity of the CXB and therefore I_{obj} is not affected by the possible uncertainties which could affect the estimate of the CXB.

The LogN(>S)–LogS best fit model implies the saturation of the 2-10 keV CXB at a flux of $\sim 8.7 \times 10^{-15}$ ergs cm^{-2} s^{-1} . Therefore deeper X-ray surveys in this energy range (e.g. the SAX, Jet-X and XMM deep surveys) should find a flattening of the number-flux relationship in the range $\sim 8.7 \times 10^{-15}$ – $\sim 6.3 \times 10^{-14}$ ergs cm^{-2} s^{-1} , i.e. within a factor $\sim$ 10

from the present flux limit.

4. Discussion and conclusion

It is clear that a decisive and final understanding of the real nature of the hard X-ray sources in this sample must await their spectroscopic identification.

In the meantime we can infer useful information on their nature by comparing the measured 2-10 keV LogN(>S)–LogS with that extrapolated from the soft energy band and with the predictions obtained from population synthesis models.

In figure 3 we display the LogN(>S)–LogS obtained in this work along with: a) the soft (0.5-2.0 keV) LogN(>S)–LogS (Hasinger et al., 1993) extrapolated to the 2-10 keV energy band assuming a power law spectral model with energy indices equal to 1, 0.7, 0.4 and 0.2 (dotted lines); and b) the prediction of the Comastri et al., (1995) model which is based on the Unification scheme of the AGNs (solid line).

We will discuss these two comparisons and their implications in turn.

The first comparison clearly shows a well known problem (see e.g. Warwick and Stewart, 1989): if we estimate the hard X-ray LogN(>S)–LogS by extrapolating the soft X-ray LogN(>S)–LogS and using the mean spectral properties of the sources, as determined in the soft (0.5 – 2.0 keV) energy band ($\alpha \sim 0.7-1.2$, see e.g. Almaini et al., 1996), we fail to reproduce it. In particular we predict a surface density, at a flux of the order of 10^{-13} ergs cm^{-2} s^{-1} , which is at least a factor ~ 2 less than the observed one.

If the same sources are responsible for both the soft and the hard X-ray LogN(>S)–LogS, their average spectral energy index should be of the order of 0.3.

Since at fluxes brighter than $\sim 10^{-13}$ ergs cm^{-2} s^{-1} the principal contribution to the source counts in the soft energy band is due to broad line AGNs (Seyfert 1 and QSOs) we should see a drastic change of their mean spectral properties going from the soft to the hard energy band. This hypothesis seems to be contradicted by the observations (see e.g. Comastri et al., 1992; Williams et al., 1992; Matsuoka and Cappi, 1996; Cappi et al., 1997).

An alternative hypothesis is that, in the hard energy band, we are selecting a population of sources which is actually undersampled in the soft X-ray surveys (e.g. the heavily absorbed AGNs in the Madau, Ghisellini and Fabian, 1994 and Comastri et al., 1995 models). In this respect it is worth noting the discovery (Ohta et al., 1996) of a type 2 QSOs at z=0.9 in an ASCA SIS observation of the Lynx field.

In particular the model of Comastri et al., (1995) is based on the X-rays properties of the Unification Scheme of AGNs: according to this model a population of absorbed and unabsorbed AGNs, when folded with the cosmological evolution properties determined in the soft X-ray energy band, is able to reproduce the shape and intensity of the CXB from several keV to $\sim$ 100 keV. As shown in figure 3 the predicted 2-10 keV LogN(>S)-LogS of Comastri et al. (1995) (reported as a solid line) in the flux range $\sim 6 \times 10^{-14}$ - $\sim 4 \times 10^{-11}$ ergs cm^{-2} s^{-1} is in very good agreement with our determination.

If this model is correct we can predict that $\sim$ 52 AGNs and $\sim$ 8 Clusters of Galaxies should be present among the 60 sources of the present sample. The expected composition of the AGNs population in this survey as a function of the intrinsic N_H is reported in Table 4. The population of AGNs X-ray emitters with intrinsic N_H in the range $10^{23} - 10^{24}$ cm^{-2} is the most interesting one: according to Comastri et al., 1995 they should produce the largest fraction of the CXB in the 2 – 100 keV energy range and should be practically invisible in soft X-ray surveys even at the faintest fluxes reachable with current and future X-ray missions.

We are planning to extend the survey by a factor of $\sim 2-3$ by analyzing all the available and suitable public GIS2 data. In the meantime we have started a program to identify the optical counterparts of the X-ray sources. The main problem with the spectroscopic follow up is the absolute accuracy of the ASCA attitude solution ($\sim 2'$). Fortunately ROSAT PSPC data are available for most of the selected GIS2 fields, allowing us to greatly reduce the X-ray errors circle for many of the X-ray sources associated with unabsorbed AGN and with clusters of galaxies. A comparison of the ASCA and ROSAT spectra of the selected sources with that of the CXB is in progress and will be published elsewhere.

We are grateful to A.Comastri, M.Cappi, G.Ghisellini and A. Wolter for stimulating discussions. We thank the anonymous referee for the carefull reading of the manuscript and for useful comments.

REFERENCES

Almaini, O., Shanks, T., Boyle, B.J., Griffiths, R.E., Roche, N., Stewart, G.C., and Georgantopoulos, I., 1996, MNRAS, 282, 295.

Boyle, B. J., Griffiths, R. E., Shanks, T., Stewart, G. C. & Georgantopoulos, I., 1993, MNRAS, 260, 49.

Boyle, B. J., Shanks, T., Georgantopoulos, I., Stewart, G. C. & Griffiths, R. E., 1994, MNRAS, 271, 639.

Boyle, B.J., McMahon,R.G., Wilkes, B.J., & Elvis, M., 1995, MNRAS, 272, 462.

Branduardi-Raymont et al., 1994, MNRAS, 270, 947.

Butcher, J.A., et al., 1997, MNRAS, in press.

Cappi, M., Matsuoka, M,., Comastri, A., Brinkmann, W., Elvis, M., Palumbo, G.G.C., & Vignali, C., 1997, Ap.J., 478, 492.

Comastri, A., Setti, G., Zamorani, G., Elvis, M., Giommi, P., Wilkes, B.& McDowell, J.C., 1992, Ap.J., 384, 62.

Comastri, A., Setti, G., Zamorani, G. & Hasinger, G., 1995, A&A, 296, 1.

Fabian, A.C., 1989, in "Proc. 23rd ESLAB Symp. - 2. AGN and the X-ray Background", ESA SP-296, 1097.

Fabian, A.C., & Barcons, X., 1992, ARAA, 30, 429.

Georgantopoulos, I., Stewart, G.C., Blair, A.J., Shanks, T., Griffiths, R.E., Boyle, B.J., Almaini, O., & Roche, N., 1997, MNRAS, in press.

Giacconi, R., Gursky, H., Paolini, F. & Rossi, B., 1962, Phys. Rev. Lett. 9, 439.

Gioia, I., Maccacaro, T., Schild, R., Wolter, A., Stocke, J.T., Morris, S.L., & Henry, J.P., 1990, ApJS, 72, 567.

Griffiths, R. E. & Padovani, P., 1990, Ap.J., 360, 483.

Griffiths, R. E., Georgantopoulos, I., Boyle, B. J., Stewart, G. C., Shanks, T. & Della Ceca, R., 1995, MNRAS, 275, 77.

Griffiths, R. E., Della Ceca, R., Georgantopoulos, I., Boyle, B. J., Stewart, G. C., Shanks, T. & Fruscione, A.,1996, MNRAS, 281, 71.

Gruber, D.E., 1992, in "X-ray Background" , ed. X. Barcons & A. C. Fabian (Cambridge: Cambridge Univ. Press), p.44.

Hasinger, G., 1996, MPE REP. 263, 291.

Hasinger, G., Burg, R., Giacconi, R., Hartner, G.,Schmidt, M., Trumper, J., & Zamorani, G., 1993, A&A, 275, 1.

Ikebe, Y., Ishisaki, Y., Kubo, H., Idesawa, E., Takahashi, T., Makishima, K., & Gis Team, 1995, in ASCA News, No.3, Goddard Space Flight Centre, 13.

Inoue, H., Kii, T., Ogasaka, Y., Takahashi, T., & Ueda, Y., 1996, MPE REP. 263, 323.

Jones, L.R., et al., 1997, MNRAS, in press.

Kondo, H., 1991, Ph.D. Thesis Univ. of Tokyo.

Kubo, H., Ikebe, Y., Makishima, K. & il GIS Team, 1994, in ASCA News, No.2, Goddard Space Flight Centre, 14.

Maccacaro, T. et al., 1994, Astroph. letters & comm., 29, 267.

Madau, P., Ghisellini, G. & Fabian, A.C., 1994, MNRAS, 270, L17.

Marshall, F. et al., 1980, ApJ, 235, 4.

Mather, J.C., et al., 1994 Ap.J., 420, 439.

Matsuoka, M., & Cappi, M., 1996, Mem.S.A.It., 67, 493.

Ohta, K., Yamada, T., Nakanishi, K., Ogasaka, Y., Kii, T., and Hayashida, K., 1996, Ap.J., 458, L57.

Piccinotti, G., et al., 1982, Ap.J., 253, 485.

Primini, F. A., Murray, S. S., Huchra, J., Schild, R. & Burg, R., 1991, ApJ, 374, 440.

Rosati, P., Della Ceca, R., Burg, R., Norman, C. & Giacconi, R., 1995, Ap.J., 445, L11.

Setti, G. & Woltjer, L., 1989, A&A, 224, L21.

Setti, G., & Comastri, A., 1996, IAU Symp., 168, 263.

Serlemitsos P. J. et al., 1995, PASJ, 47, 105.

Shanks, T., Georgantopoulos, I., Stewart, G. C., Pounds, K. A., Boyle, B. J. & Griffiths, R. E., 1991, Nature, 353, 315.

Stocke, J. T. et al., 1991, ApJS, 76, 813.

Tanaka, Y., Inoue, H. & Holt, S. S., 1994, PASJ, 46, L37.

Vikhlinin, A., Forman, W., Jones, C., & Murray, S., 1995, ApJ, 451, 553.

Williams, O.R., Turner, M.J.L., Stewart, G.C., et al., 1992, Ap.J., 389, 157.

Warwick, R., & Stewart, G., 1989, in "Proc. 23rd ESLAB Symp. -2. AGN and the X-ray Background", ESA SP-296, 727.

Zdziarski, A. A., Zycki, P. T., Svensson, R. & Boldt, E., 1993, Ap.J., 405, 125.

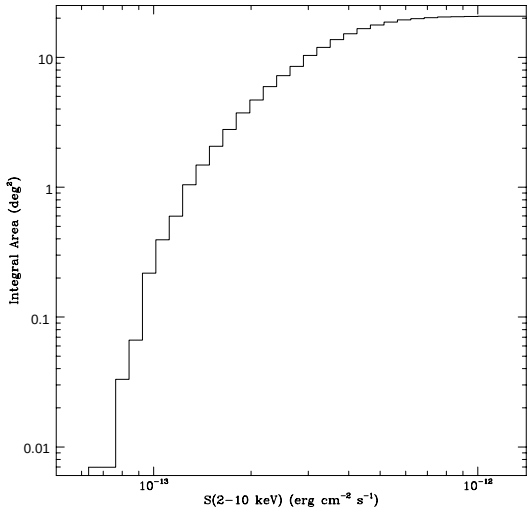

Fig. 1.— Integral sky-coverage of the present survey (see text for details).

This 2-column preprint was prepared with the AAS LaTeX macros v4.0.

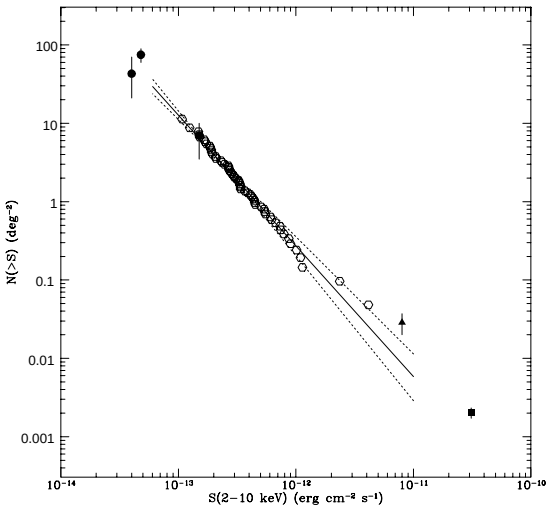

Fig. 2.— Non-parametric (open circles) representation of the number-flux relationship obtained with the selected sample. The parametric representation (solid line) is well described by a power law model, N(>S) = K $\times S^{-\alpha}$, with best fit value for the slope of $\alpha = 1.67 \pm 0.18$ and K = 2.85×10^{-21} deg^{-2}. The dotted lines represent the ±68% confidence intervals on the slope. The filled square represents the extragalactic surface density in the Piccinotti et al., 1982 sample, corrected for the 20% excess of sources due to the local superclusters (as estimated by Comastri et al., 1995). The filled triangle represents the results obtained by Kondo et al., 1991 using Ginga data. The filled dots are preliminary results in ongoing ASCA survey program conducted on a more limited sky area (Inoue et al., 1996; Georgantopoulos et al., 1997)

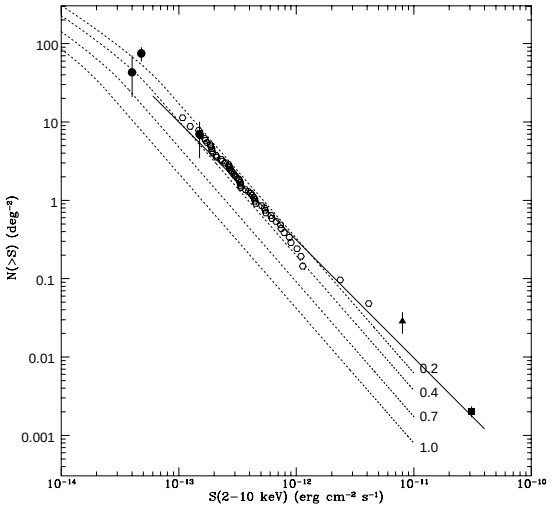

Fig. 3.— Comparison of the derived LogN(>S)-LogS (open circles) with the soft (0.5 – 2.0 keV) LogN(>S)-LogS (Hasinger et al., 1993) extrapolated in the 2–10 keV energy band assuming a power law spectral model with energy indices equal to 1, 0.7, 0.4 and 0.2 (dotted lines) The solid line represents the prediction of the Comastri et al. (1995) model.

TABLE 1
LIST OF ASCA FIELDS USED

Target Name	ROR	α [a]	δ [a]	$T_{\rm exp}$ (s)
BETA CET	21019000	00:43:37.0	−18:03:56	19977
GSGP4	92005000	00:57:29.8	−27:37:20	36934
GRB191178	22034000	01:18:40.2	−28:39:14	27160
NGC 507	61007000	01:23:03.3	+33:20:00	37591
NGC 720	60004000	01:53:19.0	−13:42:27	34213
MRK 1040	72016000	02:28:23.0	+31:22:15	19853
PHL 1377	72031000	02:35:17.9	−03:57:21	31683
AO 0235+164	71015020	02:38:30.0	+16:32:02	24858
ABELL 370	80010000	02:39:58.5	−01:31:57	34812
NGC1097	61001000	02:46:04.6	−30:18:01	36872
NGC1313	60028000	03:18:25.9	−66:28:24	23282
NGC1316	61002000	03:22:25.3	−37:14:18	34007
1H0323+022	71034000	03:26:06.2	+02:20:43	34584
EPSILON ERI	22009000	03:33:04.8	−09:24:12	19459
QSF3	90011000	03:41:44.7	−44:07:06	22967
MS0353.6-364	82042000	03:55:47.7	−36:32:12	17864
VW HYI	31001000	04:09:59.1	−71:21:03	12132
NGC1614	61011000	04:33:49.7	−08:39:08	32957
PKS0438-436	70010000	04:40:22.0	−43:32:29	32569
NGC 1667	71032000	04:48:27.0	−06:23:43	38173
E0449-184	71033000	04:51:27.0	−18:23:20	36489
MSS0451.6-03	81025000	04:54:01.2	−03:05:33	52439
MS0451.5+02	82041000	04:54:26.4	+02:54:58	18684
NGC 1808	71031000	05:07:27.7	−37:35:17	32750
MKN 3	70002000	06:15:25.3	+71:01:53	27640
0716+714	71006020	07:20:59.8	+71:17:46	19020
YY GEM	20002000	07:34:57.8	+31:57:55	30441
PI1 UMA	21018000	08:39:41.5	+65:05:16	24336
Lynx Field	90009010	08:49:11.3	+44:50:08	39943
IRAS 09104	71002000	09:13:52.6	+40:56:14	38492
GL 355	21020000	09:32:46.3	−11:09:37	19166
NGC 2992	71049000	09:45:26.2	−14:22:52	25914
NGC3079	60000000	10:01:12.4	+55:38:07	38704
3C234	71043000	10:01:27.8	+28:45:12	16194
A963	80000000	10:16:32.6	+39:00:12	23077
NGC 3147	60040000	10:17:06.4	+73:23:25	36120
AD LEO	20006000	10:19:18.7	+19:53:44	26183
IRASF10214+4	61003000	10:25:03.1	+47:10:34	34854
RE1034+39	72020000	10:35:04.3	+39:40:29	28345
NGC_3310	61013000	10:38:11.3	+53:29:19	17648
LOCKMAN HOLE	90010020	10:52:08.6	+57:22:39	21593
A1204	82002000	11:12:50.6	+17:32:40	27692
NGC 3628	61015000	11:20:31.0	+13:34:19	21616
HCG51	82028000	11:22:06.2	+24:15:02	11694
MKW4_NE	82013000	12:05:07.2	+01:57:31	19574

TABLE 1—*Continued*

Target Name	ROR	α [a]	δ [a]	$T_{\rm exp}$ (s)
NGC 4203	61008000	12:15:21.1	+33:10:22	36451
NGC_4418	62003000	12:26:35.0	+00:54:59	25875
MS1224.7+200	82043000	12:27:04.1	+19:53:02	11533
NGC4449	62011000	12:27:43.0	+44:05:25	45021
NGC 4472 NW8	60030000	12:29:23.1	+07:54:16	20128
NGC4643	62001000	12:42:52.3	+01:55:56	35222
NGC4649	61005000	12:43:54.0	+11:31:37	25447
MS1248.7+570	72032000	12:50:21.8	+56:49:13	31492
GP COM	32002000	13:05:22.3	+17:58:54	29922
NGC 4968	71039000	13:07:28.3	−23:39:01	25755
LSS_LineC-P	92002070	13:13:02.9	+31:21:36	16928
A1704	81007000	13:13:50.6	+64:38:19	18570
ABELL 1722	81013000	13:19:53.5	+70:05:20	39580
NGC5236	61016000	13:37:04.3	−29:52:08	10474
NGC5252	71021000	13:38:33.6	+04:35:08	67795
CL1358+6245	81032000	13:59:23.3	+62:35:28	35062
K416	62007000	14:05:51.4	+50:44:56	33977
PG 1404+226	72021000	14:06:07.0	+22:22:52	25639
PKS 1404-267	81019000	14:07:53.0	−26:59:12	34280
PG1407+265	70024000	14:08:54.4	+26:16:19	23344
3C295	71003000	14:11:00.0	+52:14:40	44926
MS1426.4+01	82044000	14:28:46.8	+01:46:41	18734
NGC 5695	71009000	14:37:39.8	+36:34:09	24626
HD 129333	22012000	14:38:16.6	+64:19:39	19008
NGC 5846	61012000	15:06:37.4	+01:36:39	39548
3C313	71004000	15:11:17.3	+07:54:21	41082
ARP 220	60035000	15:34:29.7	+23:27:42	33031
PG_1634+706	71036000	16:34:25.0	+70:35:27	38496
ABELL 2218	80001000	16:35:56.6	+66:15:38	23913
A2219	82037000	16:39:42.7	+46:40:27	33941
NGC6240	71022000	16:53:13.2	+02:28:15	31539
DRACO 3	90024000	17:10:24.2	+71:06:07	33590
PG_1718+481	71037000	17:19:38.6	+48:08:07	33194
NEP FIELD 1	90020000	17:59:59.8	+66:33:48	21718
PAVO_GROUP	81020000	20:18:33.1	−70:51:12	30942
PKS 2126-158	70014000	21:29:20.4	−15:34:58	11044
MS2137.3-235	81022000	21:40:29.0	−23:38:35	16794
A2440	81033000	22:23:43.2	−01:37:15	36602
PHL 5200	72033000	22:28:37.7	−05:13:42	13130
IC1459	60005000	22:57:15.6	−36:27:23	27002
DI_PEG	22002000	23:32:21.8	+15:03:11	33458
A2670	82049000	23:54:30.2	−10:19:42	27628

[a]Equatorial coordinates; equinox J2000

TABLE 3
THE LOG(N>S)-LOG(S) FIT PARAMETERS

	α	K (deg^{-2})
-90%	1.38	1.04×10^{-17}
-68%	1.49	4.45×10^{-19}
best fit	1.67	2.85×10^{-21}
$+68\%$	1.84	1.52×10^{-23}
$+90\%$	1.96	4.76×10^{-25}

TABLE 4
AGNS PREDICTED BY COMASTRI ET AL., 1995 MODEL

Log N_H (cm^{-2})	predicted AGN
< 21	26
$21 - 22$	7
$22 - 23$	11
$23 - 24$	8
$24 - 25$	< 1